Sensors and Actuators B 270 (2018) 89–96

Contents lists available at ScienceDirect

Sensors and Actuators B: Chemical

journal homepage: www.elsevier.com/locate/snb

Multiplexed analysis of molecular and elemental ions using nanowire transistor sensors

Xi Chen[a,1], Qitao Hu[a,1], Si Chen[a], Nathan L. Netzer[a,2], Zhenqiang Wang[b], Shi-Li Zhang[a], Zhen Zhang[a,*]

[a] Division of Solid-State Electronics, Department of Engineering Sciences, The Ångström Laboratory, Uppsala University, P.O. Box 534, SE-751 21 Uppsala, Sweden

[b] Department of Chemistry, The University of South Dakota, Churchill-Haines Laboratories, Room 115,414 East Clark Street, Vermillion, SD 57069-2390, United States

ARTICLE INFO

Article history:
Received 7 November 2017
Received in revised form 9 April 2018
Accepted 4 May 2018
Available online 5 May 2018

Keywords:
Elemental ion
Molecular ion
Metal-organic supercontainer
Silicon nanowire FET
ISFET
Multiplex detection

ABSTRACT

An integrated sensor chip with silicon nanowire ion-sensitive field-effect transistors for simultaneous and selective detection of both molecular and elemental ions in a single sample solution is demonstrated. The sensing selectivity is realized by functionalizing the sensor surface with tailor-made mixed-matrix membranes (MMM) incorporated with specific ionophores for the target ions. A biomimetic container molecule, named metal-organic supercontainer (MOSC), is selected as the ionophore for detection of methylene blue (MB^+), a molecular ion, while a commercially available Na-ionophore is used for Na^+, an elemental ion. The sensors show a near-Nernstian response with 56.4 ± 1.8 mV/dec down to a concentration limit of ~1 μM for MB^+ and 57.9 ± 0.7 mV/dec down to ~60 μM for Na^+, both with excellent reproducibility. Extensive control experiments on the MB^+ sensor lead to identification of the critical role of the MOSC molecules in achieving a stable and reproducible potentiometric response. Moreover, the MB^+-specific sensor shows remarkable selectivity against common interfering elemental ions in physiological samples, *e.g.*, H^+, Na^+, and K^+. Although the Na^+-specific sensor is currently characterized by insufficient immunity to the interference by MB^+, the root cause is identified and remedies generally applicable for hydrophobic molecular ions are discussed. River water experiments are also conducted to prove the efficacy of our sensors.

1. Introduction

Multiplexed analyses of liquid samples, *e.g.*, water, sweat, blood, saliva, and urine, have attracted great interest in recent years [1–5]. The liquid may consist of a complex matrix of small molecules, molecular ions, and elemental ions. Such analyses can yield rich information regarding water contaminations, individual's physiological state or early disease diagnosis. For example, the glucose level in human sweat, as an important metabolite, is closely correlated to the blood glucose level [6]. The sweat lactate is potentially a very useful early indicator of pressure ischemia [7] and lactate ion can function as a potential antioxidant agent [8]. Choline, as another example, containing a 2-Hydroxy-*N*,*N*,*N*-trimethylethan-1-aminium cation, is an essential nutrient for neurotransmission and provides methyl groups in various biological processes [9,10]. Apart from these molecular compounds, elemental ions such as Na^+ and K^+ are useful biomarkers of electrolyte imbalance and an excessive loss of them could result in dehydration [11,12]. Neurochemicals, as a further example, which also include important elemental ions (K^+, Ca^{2+}, Mg^{2+}, etc.), are actively involved in cell growth, replication, response, and communication in the neuronal network [13]. Conventional methods, such as high-performance liquid chromatography (HPLC) [14] and gas chromatography-mass spectrometry (GC–MS) [15], are widely used for quantitative measurements of these molecular ions but usually require highly-skilled operators, expensive and bulky instrumentation, and are often time consuming [16]. Electrochemical sensors have also been widely investigated [13,16,17]. However, the integration of electrochemical sensors for multiple targets onto one chip has proven to be difficult due to the different sensing mechanisms for different targets.

* Corresponding author.
E-mail address: zhen.zhang@angstrom.uu.se (Z. Zhang).
[1] The authors contributed equally to the work.
[2] Present address: Department of Natural Science, Peru State College, 600 Hoyt St. Peru, NE 68421, United States.

https://doi.org/10.1016/j.snb.2018.05.018
0925-4005/

Potentiometric sensors employing ion-binding receptors, *i.e.*, ionophores, have been extensively studied in the past decades for selective detection of cations and anions [18,19]. However, commercially available ionophores are limited to the detection of elemental and other small ions. There is a lack of ionophores for large biologically relevant molecular ions [19]. As a new class of ionophores, supramolecular host materials are becoming increasingly relevant in ion sensing applications [20]. In particular, a new class of coordination based synthetic receptors, *i.e.*, metal-organic supercontainers (MOSCs), have been proven to be an extremely efficient host system, especially for large molecular ions [21–24]. The size- and charge-selective feature of the MOSCs towards target molecular ions has been experimentally shown, with the binding affinities dependent on the molecular sizes and ionic charges of the targets [25]. It has been demonstrated in our previous work that, by incorporating MOSC molecules into poly(vinylchloride) (PVC), conventional ion-selective electrodes (ISEs) exhibited a near-Nernstian response towards methylene blue (MB^+) that has a positive charge and a molecular size closely matching the MOSC's cavity size [26]. The tunability of the nanocavity structure in the MOSCs is anticipated to afford exciting new opportunities in the potentiometric sensing of a wide range of molecular ion targets.

The success in potentiometric molecular ion sensing using a MOSC-incorporated membrane matrix offers the opportunity to integrate both molecular and elemental ion sensors in a single chip. In this work, we demonstrate an integrated sensor chip using silicon nanowire based ion-selective field-effect transistors (SiNW-ISFETs) for multiplexed analysis of molecular and elemental ions in a single sample solution. A SiNW-ISFET sensor functionalized with β-cyclodextrin (β-CD) was indeed shown to be capable of discriminating between *D* and *L* enantiomers of thyroxine [27]. Using SiNW-ISFETs for electronic sensing is advantageous due to the possibility of high-density integration as well as integration with on-chip data processing circuits [28]. Ionophore-incorporated mixed-matrix membranes (MMMs) are chosen as the ion-selective layer on the gate insulator of the SiNW-ISFETs since they have been shown to establish a more stable interface potential with the solution [18,19] than covalently functionalized ion receptors [29–31]. MB^+ is chosen as the dummy target for molecular ion sensing since its interaction with MOSC molecules has been extensively studied in the past [22,25]. A Na^+-specific sensor is constructed using the same type of polymer matrix and a commercially available Na-ionophore, as a demo elemental ion sensor. Extensive control experiments are performed for investigating the critical role of MOSCs in MMM towards stable and reproducible potentiometric responses. Considering the complexity of preforming detections in a solution that contains multiple targets, ionic interference and possible crosstalk between different sensors are necessary to be investigated. The performances of the MB^+-specific sensor with a high background concentration of elementary ions along with the Na^+-specific sensor with a high background of molecular ions are carefully examined. River water experiments are also conducted using the water from the Fyris River (Sweden) to further prove the practical utility of the SiNW-ISFET based sensors. Finally, multiplexed detection of molecular and elemental ions in one solution is demonstrated.

2. Materials and methods

2.1. Reagents and materials

The MOSC (1-Co), synthesized following a published procedure [23], was chosen for this study. Na-ionophore III (N, N, N′, N′-Tetracyclohexyl-1, 2-phenylenedioxydiacetamide), Tetrahydrofuran (THF), Bis(2-ethylhexyl)sebacate (DOS), high molecular weight poly(vinylchloride) (PVC), potassium tetrakis(4-chlorophenyl) borate (KTpClPB), KCl and NaCl were purchased from Sigma-Aldrich and used without any further purification. HCl was purchased from BASF and methylene blue (MB) from Merck Millipore. All concentration series were prepared using deionized (DI) water (18.2 MΩ cm) and the Fyris River water to reach the target value.

Table 1
Compositions for MMMs prepared in this study.

Composition	MB^+-MMM1	MB^+-MMM2	Na^+-MMM	Control-MMM
1-Co	25.7 mg			
Na-ionophore III			10 mg	
KTpClPB	5.0 mg	5.0 mg	4.5 mg	4.5 mg
PVC	330 mg	330 mg	165 mg	165 mg
THF	~5 mL	~5 mL	~5 mL	~5 mL
DOS	722 μL	722 μL	361 μL	361 μL
MB	3.2 mg	3.2 mg		

2.2. Device fabrication

The SiNW-ISFET chips were fabricated as reported previously [32] using standard silicon process technology on silicon-on-insulator wafers (SOI). In brief, the silicon layer in the channel region was thinned down from 260 to 40 nm via thermal oxidation. SiNWs were first defined by lithography and dry etching. They were then laterally shrunk to the desired width using wet etching that is selective against surrounding SiO_2 and has an etch rate highly dependent on crystal orientation [32]. To reduce the series resistance, PtSi/p^+-Si leads were used for connecting the SiNW-ISFETs to the contact pads placed at the edges of the chip. Finally, a fresh thin silicon oxide (SiO_2) film was grown via rapid thermal oxidation to serve as gate insulator and on-chip passivation.

2.3. Preparation of MMMs

Four types of MMMs were prepared: MOSC-doped MMM premixed with MB (MB^+-MMM1), MMM premixed with MB but without MOSC (MB^+-MMM2), Na-ionophore doped MMM (Na^+-MMM), and blank control MMM containing only ionic sites (Control-MMM). Detailed compositions for the four different MMMs are listed in Table 1. The preparation procedure for MB^+-MMM1 and MB^+-MMM2 can be found in our previous work [26], while that of Na^+-MMM is available in the literature [32].

Once the solution was prepared and there were no visible particles, the MMMs were fabricated by drop casting the solution on the device area of the chips by pipettes. Then, the chips with MB^+-MMM1 and MB^+-MMM2 were placed in a fume hood for approximately 2 h while the chips with Na^+-MMM were left in ordinary atmosphere overnight. Before any measurement was performed, the chips with MB^+-MMM1 and MB^+-MMM2 were conditioned in a 10 μM MB solution overnight while the chips with Na^+-MMM were conditioned in a 100 mM NaCl solution for 4 h. All procedures of MMM preparation and conditioning were conducted at room temperature.

2.4. Electrical measurement

All electrical measurements were performed at room temperature on a probe-station using a Keysight B1500A precision semiconductor parameter analyzer. To facilitate measurement with electrolyte, a polydimethylsiloxane (PDMS) container was placed on the chip. During the measurement, the gate potential (V_G) was kept constant and was applied to an Ag/AgCl reference electrode (with 3.4 M KCl as filling electrolyte, purchased from Har-

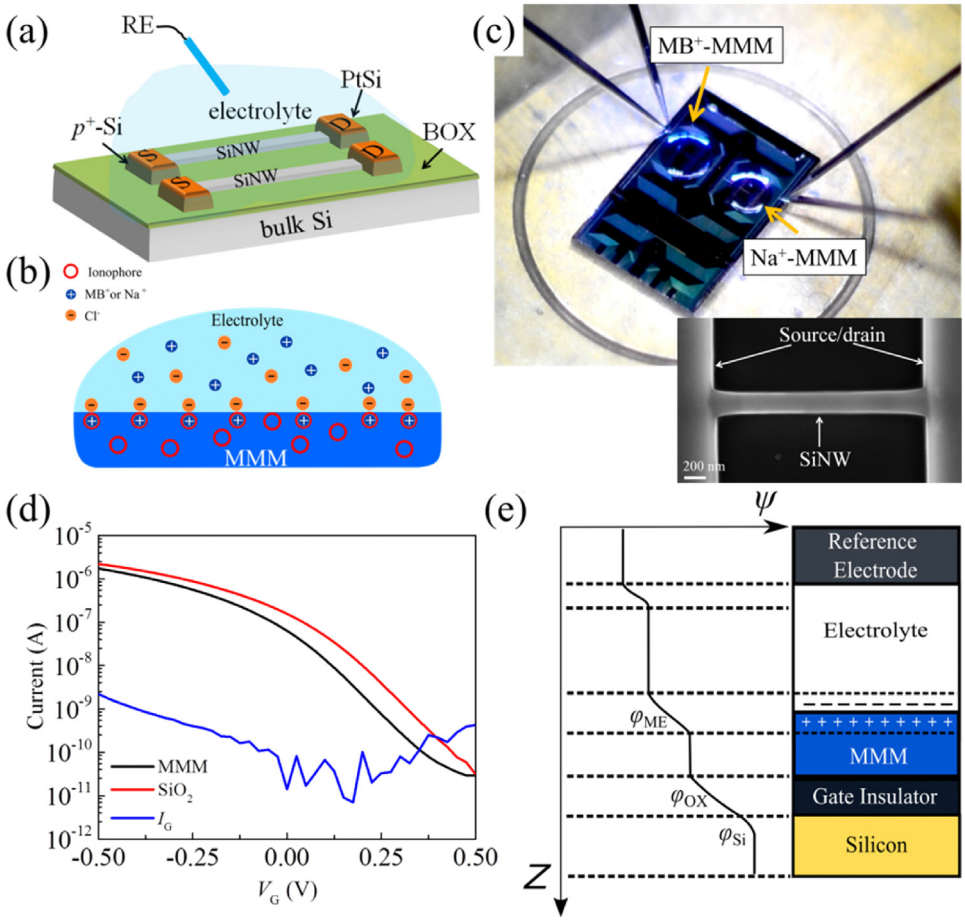

Fig. 1. (a) Three-dimensional sketch of SiNW-ISFETs covered by electrolyte, (b) a zoom-in schematic showing the charge separation and equilibrium at the MMM/electrolyte interface, (c) photo picture of our chip showing SiNW-ISFETs with MB^+-MMM (left) and Na^+-MMM (right) formed by drop-casting, insert: SEM micrograph of an SiNW-ISFET, (d) I_{DS}-V_G transfer characteristics of representative SiNW-ISFETs with and without MMM measured in electrolyte (1 mM KCl), and (e) potential distribution in the SiNW-ISFET with MMM on the gate insulator.

vard Apparatus) immersed in the solution. A three-dimensional schematic of SiNW-ISFETs covered by electrolyte is presented in Fig. 1a, followed by a zoom-in view of MMM/electrolyte interface (Fig. 1b) showing the charge separation and equilibrium at the interface. Fig. 1c shows the experimental arrangement for multiplexed detection. The SiNW-ISFET was biased in its subthreshold region. The drain-to-source current (I_{DS}) was monitored in real-time with a constant V_{DS} = 1 V. Solution exchanges during the measurement were realized manually using a pipette. In detail, each measurement was initiated with a solution with a low sample concentration in the PDMS container in order to set an I_{DS} baseline. Once the baseline became stable, the concentration in the container was increased by adding samples of higher analyte concentrations. Similar solution-exchange procedures were applied to the multiplexed detection, using a starting solution containing both molecular and elemental ions of low concentrations. Before we went back from high concentration to low concentration for repeating experiments, a thorough cleaning of the sensor was performed to avoid any hysteresis.

3. Results and discussion

3.1. Characterization of SiNW-ISFETs

The transfer characteristics, *i.e.*, I_{DS} vs V_G, of two SiNW-ISFETs with and without MMM measured in the same electrolyte are shown in Fig. 1d. The two SiNW-ISFETs have the same channel dimensions, *i.e.*, 2 μm in length, 200 nm in width, and 40 nm in height. Both devices exhibit similar subthreshold slope (*SS*), *i.e.*, 118 mV/dec, while surface functionalization with MMM has clearly decreased the threshold voltage (V_{TH}) from that of the device with bare gate insulator (marked SiO_2 in the figure). As shown in the potential diagram in Fig. 1e, when a reference electrode (RE) is used, the electrical potential of the electrolyte (ψ_{EL}) is fixed by V_G [33]. For the SiO_2/electrolyte interface, its potential (φ_{OE}) is determined by the pH value of the electrolyte since the reaction between H^+ in the electrolyte and the silanol groups (Si-OH) on the SiO_2 surface is mainly responsible for surface charging [28]. However, when the gate insulator is covered by MMM, the potential at the MMM/electrolyte interface (φ_{ME}) is governed by the binding affinity between the ionophores and target ions, as well as by the ionophores and ion concentrations in the MMM and the electrolyte, respectively [18,19]. Given the same type of MMM and same ionic composition in the electrolyte, φ_{ME} should remain unaltered. The observed difference in V_{TH} for the two SiNW-ISFETs is, thus, the consequence of φ_{ME} departing from φ_{OE}. The negligible change of *SS* by MMM is essential for maintaining the gate coupling efficiency and current sensitivity of the SiNW-ISFET [33]. This is due to the addition of ionic sites into MMM[19], which converts the MMM from an insulator to a conductor, leading to negligible potential drop across the MMM bulk when it is in series connection with the gate insulator as illustrated in Fig. 1e. It is worth noting that the gate leakage (I_G) is below 2 nA for V_G ranging from −0.5 to 0.5 V, and it is about 3 orders of magnitudes lower than the I_{DS} at the SiNW-ISFET work-

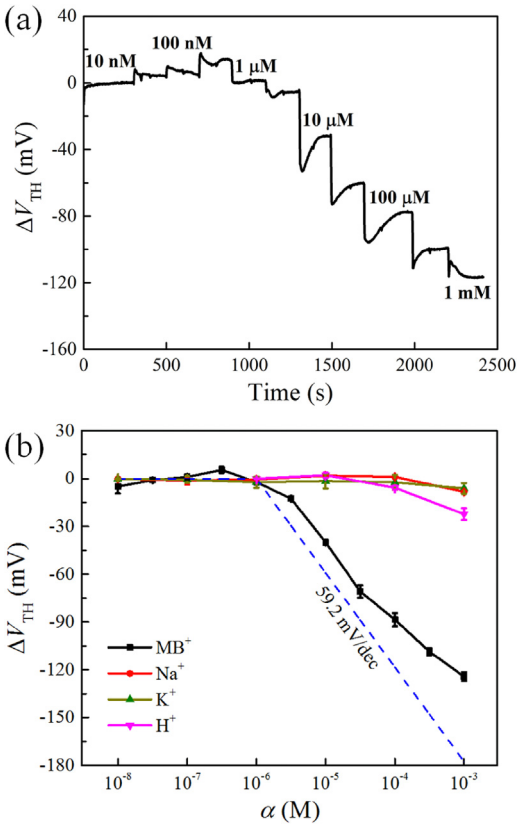

Fig. 2. ΔV_{TH} of the SiNW-ISFET functionalized with MB^+-MMM1 (a) as a function of time when α_{MB^+} was changed from low to high and (b) as a function of α_{MB^+}, including response to interfering ions such as Na^+, K^+, and H^+.

ing point, which is important for a stable sensor operation in the electrolyte.

3.2. Molecular ion sensing

The detection of MB^+ using the MB^+-MMM1 functionalized SiNW-ISFET relies on the size-selective feature of the interaction between the MOSC molecules and the MB^+ ions. The MOSC possesses one endo- (Ø ~1.7 nm) and six exo-cavities (Ø ~0.74 nm), which determines its ion-capture properties [26]. The sizes of these cavities fit nicely with the dimensions of MB^+ that measure 1.6 nm in length and 0.7 nm in width [34]. Previous work [22] has shown that 1-Co has the ability to selectively bind to MB^+ in both solution and solid-state with an apparent binding constant of $(1.42 \pm 0.31) \times 10^4\ M^{-1}$. This favorable binding is believed to be due in part to the so-called "cation-π" interaction between MB^+ and the MOSC cavity, respectively featuring a positive charge and multiple aromatic groups (aka π-systems). Fig. 2a shows ΔV_{TH} of the MB^+-MMM1 functionalized SiNW-ISFET as a function of time when the MB^+ activity, α_{MB^+}, is increased from 10 nM to 1 mM. All V_{TH} shifts are retrieved with respect to the V_{TH} value at α_{MB^+}=10 nM, *i.e.*, ΔV_{TH} = 0 mV at α_{MB^+}=10 nM. As α_{MB^+} increases, the MMM surface becomes more positively charged (and more negatively charged on the electrolyte side), leading to a negative shift of V_{TH} and lowering of I_{DS} for the SiNW-ISFET with hole conduction. The overshoot after each addition of sample solution could be related to the way of sample mixing in the PDMS container, *i.e.*, each increment of sample concentration is performed by adding a sample with higher concentration to mix with the sample already in the container. Although gently performed with the sample addition, the transport of ions and molecules in the electrolyte is governed by convection instead of diffusion [35]. This may explain the observed instantaneous response of V_{TH} to sample addition in Fig. 2a as well as the overshoot. More interface study will still be needed to validate the hypothesis. The variation of V_{TH} with α_{MB^+} is depicted in Fig. 2b, with each data point representing an average of three independent measurements. The MB^+-MMM1 functionalized SiNW-ISFET shows a near-Nernstian response to α_{MB^+} with a slope of 56.4 ± 1.8 mV/dec up to α_{MB^+}=30 μM. The change of V_{TH} starts to deviate from ideal, giving rise to a slope of 35.8 ± 1.4 mV/dec when α_{MB^+} is above 100 μM. Such a deviation at high α_{MB^+} can be explained by the co-extraction of MB^+ and Cl^- from the sample into MMM, leading to the so-called Donnan failure [19]. This can be mitigated by further optimization of the MMM composition, e.g., ratio of ionophore to ionic site [19]. The lower detection limit extrapolated from the MB+ response curve is ~1 μM. The performance of the SiNW-ISFET based MB^+ sensor is close to our MOSC-incorporated conventional ISE [26], and is also comparable with early reported MB^+ ISEs with different ion receptors and membrane compositions [36,37]. Our results prove the concept of integrating MOSC-doped MMM with SiNW-ISFET with an excellent repeatability in potentiometric MB^+ sensing. The MB^+-MMM1 functionalized SiNW-ISFET was further investigated for its response to common interfering elemental ions. As shown in Fig. 2b, no substantial shift in V_{TH} of the SiNW-ISFET is observed with α_{Na^+}, α_{K^+}, and α_{H^+} up to 100 μM. This immunity to the elemental ions is attributed to the anticipated size effect because these ions are too small in size to allow for an effective competition with the MB^+ ions for the MOSC cavities. When the ion activities were further increased from 100 μM to 10 mM, the SiNW-ISFET started to respond, giving rise to a slope of 13.2, 8.71, and 13.5 mV/dec for Na^+, K^+, and H^+, respectively. Similar responses at high ion activities (except for H^+) were also observed for the SiNW-ISFET without MMM, *i.e.*, with bare SiO_2, indicating that such responses are likely due to the response of SiO_2 to the changes of ion activities [28] in the MMM as a result of the changes in the bulk electrolyte, and are not related to the binding between the MOSC molecules and the ions. The superior selectivity against elemental ions is a clear advantage of using MOSCs for recognition of molecular ions in physiological and environmental processes.

To achieve the desired Nernstian response, it is crucial to maintain a constant activity of the ion of interest in the bulk of the membrane phase [18]. It has been shown in our previous work [26] that without MOSC molecules incorporated into the MMM, MB^+ can gradually leach into the aqueous phase, leading to a drift of α_{MB^+} in the membrane phase. Three consecutive response curves (green) of the SiNW-ISFET functionalized with such MMM without MOSC incorporation, *i.e.*, MB^+-MMM2, are depicted in Fig. 3a. The response curve (black) of the MB^+-MMM1 functionalized SiNW-ISFET is also included as a reference. Due to the instability of α_{MB^+} in the membrane phase, the sensor response deviates significantly from the ideal Nernstian behavior. Moreover, the reproducibility is poor in comparison with the reference, as evident by its substantially larger standard deviation shown in Fig. 3b. The detection limit of the MB^+-MMM2 functionalized SiNW-ISFET is also inferior to the reference, which could be explained by MB^+ leaching out from MB^+-MMM2, thereby [19] considerably raising α_{MB^+} at the interface, $\alpha^{IF}_{MB^+}$. In another case where MMM contained neither premixed ion of interest (MB^+) nor MOSC molecules, designated as Control-MMM, the sensor showed a negligible potentiometric response during the first measurement. This is expected since there was no MB^+ in the MMM to balance the charge and to establish a stable phase boundary potential with the MB^+ in the solution. However, MB^+ is relatively hydrophobic. As the SiNW-ISFET with Control-MMM is used over and over again, the MB^+ could be incorporated into the hydrophobic membrane due to the hydrophobic interactions. This renders the MMM to an ion-exchange membrane. By repeating the measurement for the second and third times, α_{MB^+}

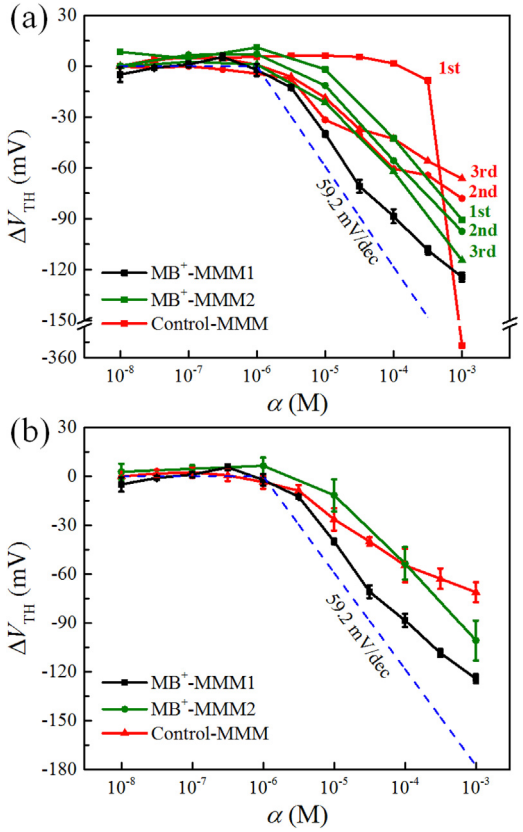

Fig. 3. ΔV_{TH} of the SiNW-ISFETs with different MMMs as a function of α_{MB^+}. In (a), three consecutive measurements for SiNW-ISFETs with MB^+-MMM2 and Control-MMM are plotted separately, and in (b) response curves averaged from three measurements.

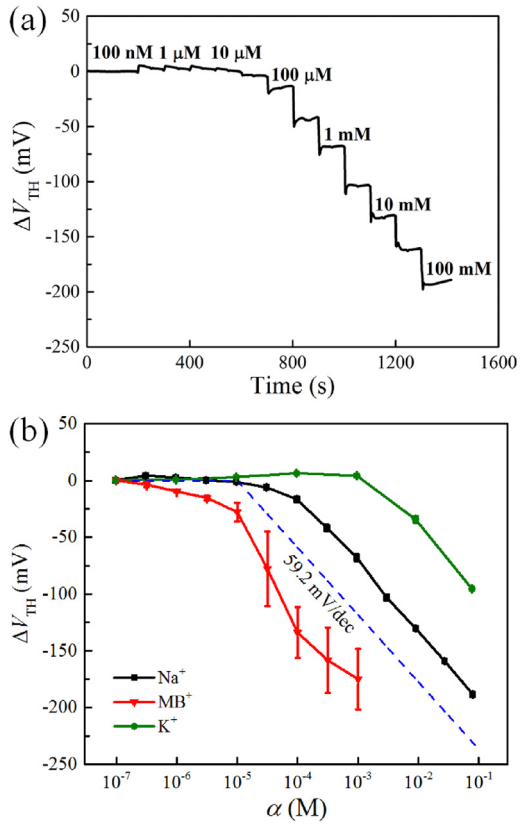

Fig. 4. ΔV_{TH} of the SiNW-ISFET functionalized with Na^+-MMM (a) as a function of time when α_{Na^+} was changed from low to high, and (b) as a function of α_{Na^+}, α_{K^+}, and α_{MB^+}. For the detection of Na^+ and MB^+, the interfering ion is K^+ with α_{K^+} =1 mM, while for the detection of K^+, the interfering ion is Na^+ with α_{Na^+} =1 mM. Error bars are shown for the Na^+ and MB^+ response curves in (b) but they are smaller than the plot markers.

in Control-MMM increases and the SiNW-ISFET sensor starts to respond with a low detection limit similar to the reference (black). However, the response curve averaged from three measurements, shown in red in Fig. 3b, significantly deviates from the ideal Nernstian behavior. Such a sub-Nernstian response could be ascribed to a sample dependent α_{MB^+} in Control-MMM [18,19], *i.e.*, α_{MB^+} is not constant in the membrane phase but is dependent on the MB^+ activity in the aqueous phase. The results here clearly demonstrate the critical role of the MOSC molecules for stabilization of the activity of the ion of interest in MMM, which is essential for achieving a Nernstian response.

3.3. Elemental ion sensing

Fig. 4a shows ΔV_{TH} of a Na^+-MMM functionalized SiNW-ISFET as a function of time with increasing α_{Na^+}. An overshot is also visible after addition of each new sample solution but the recovery is significantly faster than observed in MB^+ sensing, which could be explained by the relatively higher diffusivity of Na^+ comparing to the bulkier MB^+ in the solution and thus shorter time for the solution to become homogenized. As depicted in Fig. 4b, in the presence of K^+ as a likely interfering ion with α_{K^+}=1 mM, the Na^+-MMM functionalized SiNW-ISFET exhibits a near-Nernstian response with a slope of 57.9 ± 0.7 mV/dec in a wide α_{Na^+} range from 100 μM to 100 mM, with a lower detection limit of ~60 μM. Such a performance is in close match with the reported data obtained from a conventional ISE with the same Na-ionophore [38], and is better than the recently demonstrated SiNW-FET based Na^+ sensor [30]. On the other hand, the response to K^+, in the presence of Na^+ as a likely interfering ion with α_{Na^+}=1 mM, becomes close to Nernstian (~61 mV/dec) at much higher concentrations, *i.e.*, α_{K^+} > 10 mM.

A selectivity coefficient $K^{Pot}_{Na,K}$ of $10^{-1.2}$ can be estimated from the lower detection limit of Na^+ (α_{Na^+}(DL)) in the presence of interfering K^+ with an activity of α_{K^+} through [19]:

$$\alpha_{Na^+}(DL) = K^{Pot}_{Na,K}\alpha_{K^+}, \quad (1)$$

which is in good agreement with the reported values [32,38,39].

Considering the abundance of molecular ions in physiological samples, it is important to investigate the cross-sensitivity of the elemental ion sensor towards molecular ions. The response curve of the Na^+-MMM functionalized SiNW-ISFET towards the molecular ion MB^+ is shown in Fig. 4b. Similar to the case of Control-MMM, the hydrophobic MB^+ is likely incorporated into the Na^+-MMM during measurement. The SiNW-ISFET exhibits a super-Nernstian response towards MB^+ once α_{MB^+} is above a critical threshold, *i.e.*, ~10 μM in this experiment, with a large standard deviation among the measurements. Therefore, in order to have a controllable detection of elemental ions, it is essential to keep the activity of hydrophobic ions below the threshold at which they start to be incorporated into MMM.

3.4. Detections with river water

To show that our sensors could be utilized for more practical and complex samples, both molecular and elemental ion detection experiments were performed with the water collected from the Fyris River in the city of Uppsala, Sweden. The response curves of the MB^+-MMM1 functionalized SiNW-ISFET are undistinguishable between the river water and the DI water as depicted in Fig. 5. These results clearly demonstrate the robustness of the SiNW-ISFET

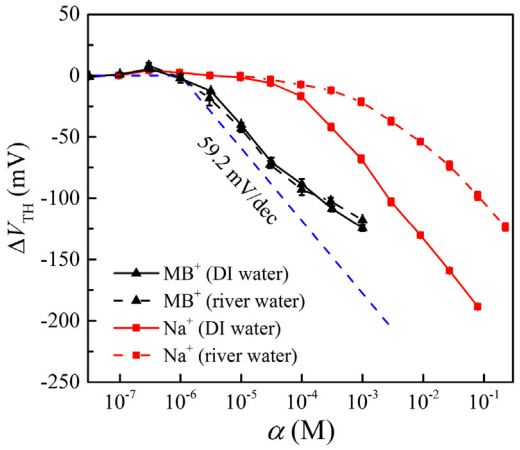

Fig. 5. ΔV_{TH} of the SiNW-ISFETs functionalized with MB^+-MMM1 and Na^+-MMM as a function of α_{MB^+} and α_{Na^+}, respectively, with a concentration series prepared using DI water and river water.

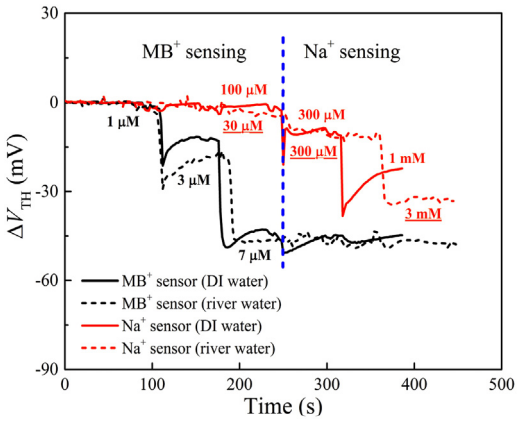

Fig. 6. Multiplexed measurement of MB^+ (black) and Na^+ (red) in one solution with the concentration series prepared with DI water (solid line) and river water (dash line). The MB^+-sensor is functionalized with MB^+-MMM1 and the Na^+-sensor is functionalized with Na^+-MMM. The same α_{MB^+} range is applied for MB^+ detections with the DI and river waters. For Na^+ detections, larger α_{Na^+} steps are used with the river water (α_{Na^+} with underline). (For interpretation of the references to colour in this figure legend, the reader is referred to the web version of this article.)

based molecular ion sensor, which can be attributed to its remarkable selectivity against interfering elemental ions often abundantly present in river water. Similar experiments were conducted with the Na^+-MMM functionalized SiNW-ISFET. Significant performance deterioration is observed as evident by a sub-Nernstian response and an increase of the lower detection limit in Fig. 5. This behavior can result from the presence of a multiple of other elemental ions in the river water [40], *e.g.*, K^+ and Ca^{2+}, that interfere with the Na^+ detection [32,39]. Nevertheless, the slope of the response curve improves with increasing α_{Na^+}, reaching 54.5 ± 0.9 mV/dec when α_{Na^+} is above 30 mM, as a result of the reduced effect from the interfering ions at high analyte concentrations.

3.5. Multiplexed analysis

Finally, the MB^+-specific and Na^+-specific SiNW-ISFET sensors are integrated on the same chip, as the demonstrator of a multiplexed analysis of molecular and elemental ions in one solution. The two MMMs are manually coated onto the sensors by drop casting. As shown in the previous section, the hydrophobic MB^+ will be extracted from the solution into the Na^+-MMM, giving rise to false response on the Na^+-specific sensor. As a result, α_{MB^+} in the solution is kept below the threshold, *i.e.*, 10 μM, during this demonstration. As shown in Fig. 6, when the experiment is conducted with DI water, α_{MB^+} in the solution is first increased from 1 to 3 μM and then from 3 to 7 μM, the MB^+-specific sensor shows ΔV_{TH} of 12.5 and 30.7 mV, respectively. This is in good agreement with previously demonstrated response shown in Fig. 2b. With these changes, V_{TH} of the Na^+-specific senor remains unaltered. Afterwards, α_{Na^+} in the solution is increased from 100 to 300 μM and then from 300 μM to 1 mM, the corresponding ΔV_{TH} of the Na^+-specific sensor is 9.4 and 13.0 mV; both are relatively small in comparison with the data obtained from the separate solution measurements as shown in Fig. 4b. This could be due to the use of a higher concentration of KCl, *i.e.*, 10 mM, as the background electrolyte in this demonstration, since K^+ is a strong interfering ion for the Na^+-specific sensor. A slower process to restore the interface equilibrium after the overshot is observed in Na^+ sensing than observed in Fig. 4a, which is possibly due to the involvement of MB^+. When the experiment is conducted with the river water, the same α_{MB^+} range as with DI water is applied since the MB^+-specific sensor produces similar response curves in both water solutions. On the other hand, larger α_{Na^+} steps are used due to the performance deterioration of the Na^+-specific sensor with the river water. As expected, the MB^+-specific sensor shows ΔV_{TH} of 18.0 and 28.5 mV with the increase of α_{MB^+} first from 1 to 3 μM and then from 3 to 7 μM, respectively, while the Na^+-specific sensor shows no detectable ΔV_{TH}. Afterwards, α_{Na^+} in the solution is increased from 30 to 300 μM and then from 300 μM to 3 mM, the corresponding ΔV_{TH} of the Na^+-specific sensor is 6.4 and 22.5 mV.

Our results demonstrate the possibility to operate the two types of sensors targeting, with high specificity, both molecular and elemental ions simultaneously in a complex sample. It is worth noting that cross-interference issues are also identified. Follow-up investigations will be performed with the goal both to enlarge the detection range and to improve the voltage sensitivities for multi-targets.

4. Conclusions

We have demonstrated an integrated SiNW-ISFET based sensor chip for multiplexed analysis of both molecular and elemental ions in a single sample solution. A same polymer matrix is used to form the ion-selective membranes in both types of sensors to greatly simplify the integration process. When used separately, the sensors show a near-Nerstian response in wide concentration ranges. The molecular ion sensor further shows excellent selectivity against common interfering elemental ions, e.g., H^+, Na^+, and K^+. In contrast, the elemental ion sensor is shown to be more susceptible to the presence of molecular ions due to the partitioning of relatively more hydrophobic molecular ions into MMM. Based on the understanding of cross-interfering mechanism of the two types of sensors, we have demonstrated simultaneous and selective detection of molecular and elemental ions in a single sample solution, as long as the activity of the molecular ions in the solution is kept below a critical threshold. To demonstrate the practical utility of our sensors, multiplexed sensing experiments have also been demonstrated with the water from the Fyris River (Sweden). Further engineering of MMM in the elemental ion sensor to enable effective shielding of hydrophobic ions will be essential for applications of such a platform for multiplexed analysis of real-life, complex samples.

Acknowledgments

This work was supported by the Swedish Strategic Research Foundation (SSF ICA 12-0047 and FFL15-0174), the Swedish Research Council (VR 2014-5588), Göran Gustafssons Foundation

(GG 1459B), Carl Tryggers Foundation (CTS14-527), and the Wallenberg Academy Fellow Program. The work related to the MOSC synthesis, characterizations, and ion sensing was supported by NSF grants CHE-1352279 (Z.W.) and DMR-1709912 (Z.W. & N.L.N.)

References

[1] V. Gubala, L.F. Harris, A.J. Ricco, M.X. Tan, D.E. Williams, Point of care diagnostics: status and future, Anal. Chem. 84 (2012) 487–515, http://dx.doi.org/10.1021/ac2030199.
[2] W. Gao, S. Emaminejad, H.Y.Y. Nyein, S. Challa, K. Chen, A. Peck, H.M. Fahad, H. Ota, H. Shiraki, D. Kiriya, D.-H. Lien, G.A. Brooks, R.W. Davis, A. Javey, Fully integrated wearable sensor arrays for multiplexed in situ perspiration analysis, Nature 529 (2016) 509–514, http://dx.doi.org/10.1038/nature16521.
[3] P.N. Floriano, N. Christodoulides, C.S. Miller, J.L. Ebersole, J. Spertus, B.G. Rose, D.F. Kinane, M.J. Novak, S. Steinhubl, S. Acosta, S. Mohanty, P. Dharshan, C. Yeh, S. Redding, W. Furmaga, J.T. McDevitt, Use of saliva-Based nano-Biochip tests for acute myocardial infarction at the point of care: a feasibility study, Clin. Chem. 55 (2009) 1530, http://dx.doi.org/10.1373/clinchem.2008.117713.
[4] J.M. Klostranec, Q. Xiang, G.A. Farcas, J.A. Lee, A. Rhee, E.I. Lafferty, S.D. Perrault, K.C. Kain, W.C.W. Chan, Convergence of quantum dot barcodes with microfluidics and signal processing for multiplexed high-Throughput infectious disease diagnostics, Nano Lett. 7 (2007) 2812–2818, http://dx.doi.org/10.1021/nl071415m.
[5] G. Davis, I.R., Lauks, C., Lin, C.J. Miller, Apparatus and methods for analyte measurement and immunoassay, U.S. Patent 8,017,382, 2011. http://www.google.com/patents/US8017382.
[6] J. Moyer, D. Wilson, I. Finkelshtein, B. Wong, R. Potts, Correlation between sweat glucose and blood glucose in subjects with diabetes, Diabetes Technol. Ther. 14 (2012) 398–402, http://dx.doi.org/10.1089/dia.2011.0262.
[7] S.L. Knight, R.P. Taylor, A.A. Polliack, D.L. Bader, Establishing predictive indicators for the status of loaded soft tissues, J. Appl. Physiol. 90 (2001) 2231.
[8] C. Groussard, I. Morel, M. Chevanne, M. Monnier, J. Cillard, A. Delamarche, Free radical scavenging and antioxidant effects of lactate ion: an in vitro study, J. Appl. Physiol. 89 (2000) 169–175.
[9] M.B. Glier, T.J. Green, A.M. Devlin, Methyl nutrients, DNA methylation, and cardiovascular disease, Mol. Nutr. Food Res. 58 (2014) 172–182, http://dx.doi.org/10.1002/mnfr.201200636.
[10] R. Schliebs, T. Arendt, The cholinergic system in aging and neuronal degeneration, Behav. Brain Res. 221 (2011) 555–563, http://dx.doi.org/10.1016/j.bbr.2010.11.058.
[11] D.B. Speedy, T.D. Noakes, C. Schneider, Exercise-associated hyponatremia: a review, Emerg. Med. 13 (2001) 17–27, http://dx.doi.org/10.1046/j.1442-2026.2001.00173.x.
[12] M.F. Bergeron, Heat cramps: fluid and electrolyte challenges during tennis in the heat, J. Sci. Med. Sport. 6 (2003) 19–27, http://dx.doi.org/10.1016/S1440-2440(03)80005-1.
[13] T. Xiao, F. Wu, J. Hao, M. Zhang, P. Yu, L. Mao, In vivo analysis with electrochemical sensors and biosensors, Anal. Chem. 89 (2017) 300–313, http://dx.doi.org/10.1021/acs.analchem.6b04308.
[14] P. Uutela, R. Reinilä, P. Piepponen, R.A. Ketola, R. Kostiainen, Analysis of acetylcholine and choline in microdialysis samples by liquid chromatography/tandem mass spectrometry, Rapid Commun. Mass Spectrom. 19 (2005) 2950–2956, http://dx.doi.org/10.1002/rcm.2160.
[15] T.A. Patterson, J.W. Kosh, Simultaneous quantitation of arecoline, acetylcholine, and choline in tissue using gas chromatography/electron impact mass spectrometry, Biol. Mass Spectrom. 21 (1992) 299–304, http://dx.doi.org/10.1002/bms.1200210606.
[16] N. Chauhan, J. Narang, U. Jain, Highly sensitive and rapid detection of acetylcholine using an ITO plate modified with platinum-graphene nanoparticles, Analyst 140 (2015) 1988–1994, http://dx.doi.org/10.1039/C4AN01873G.
[17] M. Labib, E.H. Sargent, S.O. Kelley, Electrochemical methods for the analysis of clinically relevant biomolecules, Chem. Rev. 116 (2016) 9001–9090, http://dx.doi.org/10.1021/acs.chemrev.6b00220.
[18] P. Bühlmann, L.D. Chen, Ion-Selective electrodes with ionophore-Doped sensing membranes, in: Supramol Chem., John Wiley & Sons, Ltd, 2012, http://dx.doi.org/10.1002/9780470661345.smc097.
[19] E. Bakker, P. Bühlmann, E. Pretsch, Carrier-Based ion-Selective electrodes and bulk optodes. 1, Gen. Characteristics, Chem. Rev. 97 (1997) 3083–3132, http://dx.doi.org/10.1021/cr940394a.
[20] P. Kumar, A. Deep, K.-H. Kim, Metal organic frameworks for sensing applications, TrAC Trends Anal. Chem. 73 (2015) 39–53, http://dx.doi.org/10.1016/j.trac.2015.04.009.
[21] F.-R. Dai, Z. Wang, Modular assembly of metal–organic supercontainers incorporating sulfonylcalixarenes, J. Am. Chem. Soc. 134 (2012) 8002–8005, http://dx.doi.org/10.1021/ja300095j.
[22] F.-R. Dai, U. Sambasivam, A.J. Hammerstrom, Z. Wang, Synthetic supercontainers exhibit distinct solution versus solid state guest-Binding behavior, J. Am. Chem. Soc. 136 (2014) 7480–7491, http://dx.doi.org/10.1021/ja502839b.
[23] N.L. Netzer, F.-R. Dai, Z. Wang, C. Jiang, pH-modulated molecular assemblies and surface properties of metal–organic supercontainers at the air–water interface, Angew. Chem. Int. Ed 53 (2014) 10965–10969, http://dx.doi.org/10.1002/anie.201406733.
[24] F.-R. Dai, D.C. Becht, Z. Wang, Modulating guest binding in sulfonylcalixarene-based metal?organic supercontainers, Chem. Commun. 50 (2014) 5385–5387, http://dx.doi.org/10.1039/C3CC47420H.
[25] F.-R. Dai, Y. Qiao, Z. Wang, Designing structurally tunable and functionally versatile synthetic supercontainers, Inorg. Chem. Front. 3 (2016) 243–249, http://dx.doi.org/10.1039/C5QI00212E.
[26] N.L. Netzer, I. Must, Y. Qiao, S.-L. Zhang, Z. Wang, Z. Zhang, Biomimetic supercontainers for size-selective electrochemical sensing of molecular ions, Sci. Rep. 7 (2017) 45786.
[27] X. Duan, N.K. Rajan, D.A. Routenberg, J. Huskens, M.A. Reed, Regenerative electronic biosensors using supramolecular approaches, ACS Nano 7 (2013) 4014–4021, http://dx.doi.org/10.1021/nn306034f.
[28] P. Bergveld, Thirty years of ISFETOLOGY: What happened in the past 30 years and what may happen in the next 30 years, Sens. Actuators B Chem. 88 (2003) 1–20.
[29] L.R. Stoop, M. Wipf, S. Müller, K. Bedner, A.I. Wright, J.C. Martin, C.E. Constable, A. Fanget, C. Schönenberger, M. Calame, Implementing silicon nanoribbon field-effect transistors as arrays for multiple ion detection, Biosensors 6 (2016), http://dx.doi.org/10.3390/bios6020021.
[30] M. Wipf, R.L. Stoop, A. Tarasov, K. Bedner, W. Fu, I.A. Wright, C.J. Martin, E.C. Constable, M. Calame, C. Schönenberger, Selective sodium sensing with gold-Coated silicon nanowire field-effect transistors in a differential setup, ACS Nano 7 (2013) 5978–5983, http://dx.doi.org/10.1021/nn401678u.
[31] R.L. Stoop, M. Wipf, S. Müller, K. Bedner, I.A. Wright, C.J. Martin, E.C. Constable, W. Fu, A. Tarasov, M. Calame, C. Schönenberger, Competing surface reactions limiting the performance of ion-sensitive field-effect transistors, Sens. Actuators B Chem. 220 (2015) 500–507, http://dx.doi.org/10.1016/j.snb.2015.05.096.
[32] J.A. Brunink, J.R. Haak, J.G. Bomer, D.N. Reinhoudt, M.A. McKervey, S.J. Harris, Chemically modified field-effect transistors; a sodium ion selective sensor based on calix [4] arene receptor molecules, Anal. Chim. Acta. 254 (1991) 75–80.
[33] S. Chen, S.-L. Zhang, Contacting versus insulated gate electrode for Si nanoribbon field-effect sensors operating in electrolyte, Anal. Chem. 83 (2011) 9546–9551, http://dx.doi.org/10.1021/ac2023316.
[34] P. Simoncic, T. Armbruster, Cationic methylene blue incorporated into zeolite mordenite-Na: a single crystal X-ray study, Microporous Mesoporous Mat. 81 (2005) 87–95, http://dx.doi.org/10.1016/j.micromeso.2005.01.019.
[35] S. Chen, Z.-B. Zhang, L. Ma, P. Ahlberg, X. Gao, Z. Qiu, D. Wu, W. Ren, H.-M. Cheng, S.-L. Zhang, A graphene field-effect capacitor sensor in electrolyte, Appl. Phys. Lett. 101 (2012) 154106, http://dx.doi.org/10.1063/1.4759147.
[36] M.L. Wen, Y.B. Zhao, X. Chen, C.Y. Wang, Potentiometric sensor for methylene blue based on methylene blue–silicotungstate ion association and its pharmaceutical applications, J. Pharm. Biomed. Anal. 18 (1999) 957–961.
[37] S.S. Hassan, S.A. Marzouk, H.E. Sayour, Methylene blue potentiometric sensor for selective determination of sulfide ions, Anal. Chim. Acta. 466 (2002) 47–55.
[38] T. Maruizumi, D. Wegmann, G. Suter, D. Ammann, W. Simon, Neutral carrier-based Na+-selective electrode for application in blood serum, Microchim. Acta. 88 (1986) 331–336.
[39] J.A.J. Brunink, J.G. Bomer, J.F.J. Engbersen, W. Verboom, D.N. Reinhoudt, Effects of anionic sites on the selectivity of sodium-sensitive CHEMFETs, Sens, Actuators B Chem. 15–16 (15) (1993) 195––.
[40] WISS - Water Information System Sweden - Measuring point: Fyrisån, Flottsund, WISS - Water Inf. Syst. Swed. – Meas. Point Fyrisån Flot. (2017). http://viss.lansstyrelsen.se/Stations.aspx?stationEUID=SE663116-160415. (Accessed 9 May 2017).

Biographies

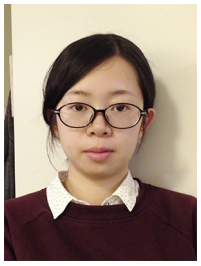

Xi Chen received the B.S. degree (2013) from University of Science and Technology of China, and is currently a Ph.D. student in solid state electronics division from Uppsala University, Sweden. Her research interests include nano-devices for sensing applications, and low frequency noise in electronic devices and electronic ion-sensors.

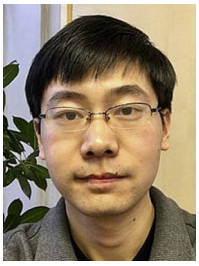

Qitao Hu received the B.S. degree (2015) from University of Science and Technology of China. He is a PhD student at solid-state electronics at Uppsala University in Uppsala, Sweden. His research topic is the ion sensor based on Si nanowire field effect transistors.

Si Chen received the B.S. degree (2004) from University of Science and Technology of China and the M.S. degree (2007) from Shanghai Institute of Ceramics, Chinese Academy of Sciences, and Ph.D. degree (2013) in solid state electronics from Uppsala University, Sweden. He worked as a characterization and development engineer at Solibro Research AB from 2013 to 2016, and joined Uppsala University in 2016 as a researcher. His main research interest is novel device structures and materials for electronic biosensor applications.

Nathan Netzer is an assistant professor of Chemistry at Peru State College, USA. He received the BSc degree (2009), MSc degree (2011) and PhD degree (2014) in chemistry from University of South Dakota in USA. He joined Uppsala University, Sweden as a postdoctoral researcher in 2015 and started his faculty position at Peru State College in 2017. His current research interests include nanoscale material synthesis, characterization, and device fabrication.

Zhenqiang Wang is an associate professor of chemistry at the University of South Dakota, USA. He received his B.S. degree (2000) from Peking University and PhD degree (2006) from the University of South Florida. He did his postdoctoral work at U.C. San Diego before joining the chemistry department at the University of South Dakota. His current research interests include porous materials for selective gas adsorption, supramolecular catalysts that activate small molecules and smart materials that respond to external stimuli.

Shi-Li Zhang is the chair professor of solid-state electronics at Uppsala University in Uppsala, Sweden. He received the BSc degree (1982) and the MSc degree (1985) both in physics from Fudan University in Shanghai, and the PhD degree (1990) in electronics from the Royal Institute of Technology (KTH) in Stockholm. His current research interests include nanodevices for genome sequencing, flexible energy devices based on 2-dimensional semiconductor materials, and energy-efficient interconnects for nano- and power electronics.

Zhen Zhang is a professor of solid-state electronics at Uppsala University in Uppsala, Sweden. He received the Ph.D degree in department of microelectronics and information technology from Royal Institute of Technology (KTH) of Sweden in 2008. He worked as a research staff member at IBM T. J. Watson research center at Yorktown Heights, New York from 2008 to 2013, and joined Uppsala University in 2013. His research interest covers semiconductor based electronic sensors, nano-scale semiconductor devices and bio-electronics.